Atmos. Meas. Tech., 2, 725–739, 2009
www.atmos-meas-tech.net/2/725/2009/
© Author(s) 2009. This work is distributed under
the Creative Commons Attribution 3.0 License.

Atmospheric Measurement Techniques

Relationship between the NO_2 photolysis frequency and the solar global irradiance

I. Trebs[1], B. Bohn[2], C. Ammann[3,1], U. Rummel[4,1], M. Blumthaler[5], R. Königstedt[1], F. X. Meixner[1], S. Fan[6], and M. O. Andreae[1]

[1]Max Planck Institute for Chemistry, Biogeochemistry and Air Chemistry Department, P.O. Box 3060, 55020 Mainz, Germany
[2]Research Centre Jülich GmbH, Institute of Chemistry and Dynamics of the Geosphere 2: Troposphere, 52425 Jülich, Germany
[3]Agroscope ART, Air Pollution and Climate Group, 8046 Zürich, Switzerland
[4]Richard Assmann Observatory Lindenberg, German Meteorological Service, Germany
[5]Medical University, Division for Biomedical Physics, Müllerstr. 44, 6020 Innsbruck, Austria
[6]Institute of Environmental Meteorology, School of Environmental Science and Engineering, Sun Yat-sen University, Guangzhou, 510275, China

Received: 4 May 2009 – Published in Atmos. Meas. Tech. Discuss.: 13 July 2009
Revised: 15 October 2009 – Accepted: 16 October 2009 – Published: 16 November 2009

Abstract. Representative values of the atmospheric NO_2 photolysis frequency $j(NO_2)$ are required for the adequate calculation and interpretation of NO and NO_2 concentrations and exchange fluxes near the surface. Direct measurements of $j(NO_2)$ at ground level are often not available in field studies. In most cases, modeling approaches involving complex radiative transfer calculations are used to estimate $j(NO_2)$ and other photolysis frequencies for air chemistry studies. However, important input parameters for accurate modeling are often missing, most importantly with regard to the radiative effects of clouds. On the other hand, solar global irradiance ("global radiation", G) is nowadays measured as a standard parameter in most field experiments and in many meteorological observation networks around the world. Previous studies mainly reported linear relationships between $j(NO_2)$ and G. We have measured $j(NO_2)$ using spectro- or filter radiometers and G using pyranometers side-by-side at several field sites. Our results cover a solar zenith angle range of 0–90°, and are based on nine field campaigns in temperate, subtropical and tropical environments during the period 1994–2008. We show that a second-order polynomial function (intercept = 0): $j(NO_2) = (1+\alpha) \times (B_1 \times G + B_2 \times G^2)$, with α defined as the site-dependent UV-A surface albedo and the polynomial coefficients: $B_1 = (1.47 \pm 0.03) \times 10^{-5}\,W^{-1}\,m^2\,s^{-1}$ and $B_2 = (-4.84 \pm 0.31) \times 10^{-9}\,W^{-2}\,m^4\,s^{-1}$ can be used to estimate ground-level $j(NO_2)$ directly from G, independent of solar zenith angle under all atmospheric conditions. The absolute $j(NO_2)$ residual of the empirical function is $\pm 6 \times 10^{-4}\,s^{-1}(2\sigma)$. The relationship is valid for sites below 800 m a.s.l. and with low surface albedo ($\alpha < 0.2$). It is not valid in high mountains, above snow or ice and sandy or dry soil surfaces.

1 Introduction

Solar ultraviolet (UV) radiation drives the photodissociation of tropospheric species and thus participates in chain-initiating reactions that play a key role for the chemistry of the troposphere. The fast photolysis of nitrogen dioxide (NO_2) largely controls tropospheric ozone (O_3) formation and, consequently, is important for the production of hydroxyl (OH) radicals, which are secondary products of ozone photolysis under tropospheric conditions (Crutzen and Lelieveld, 2001).

$$NO_2 + h\nu\,(\lambda < 420\,nm) \rightarrow NO + O\left(^3P\right) \quad \text{(R1)}$$

$$O\left(^3P\right) + O_2 + M \rightarrow O_3 + M \quad \text{(R2)}$$

Correspondence to: I. Trebs
(i.trebs@mpic.de)

Published by Copernicus Publications on behalf of the European Geosciences Union.

The first-order rate constant of reaction R1 is called the NO_2 photolysis frequency, $j(NO_2)$, which is a function of (a) the ability of the NO_2 molecule to absorb radiation (absorption cross section), (b) the probability that it is decomposed into NO and $O(^3P)$ (quantum yield), and (c) the actinic flux in the UV-A range (320–420 nm). The actinic flux is defined as the total radiative energy flux incident on a sphere having unity cross sectional area, irrespective of the beam direction. The actinic flux relevant for Reaction (R1) in the troposphere is determined by the solar radiation entering the atmosphere and modifications by Rayleigh scattering and absorptions by gaseous constituents (e.g., stratospheric O_3, tropospheric NO_2 in polluted urban areas), scattering and absorption by clouds and aerosols, and by reflections from the ground (e.g., Seinfeld and Pandis, 2006). The value of $j(NO_2)$ is therefore dependent on the solar zenith angle (SZA), the altitude, and other specific local environmental conditions.

The photolysis of NO_2 may be an important parameter affecting the surface-atmosphere exchange of NO_2 and associated reactive species, such as nitric oxide (NO) and O_3. The application of the flux-gradient method (Dyer and Hicks, 1970) and resistance based inferential models (Hicks et al., 1987) presumes that vertical exchange fluxes of the so-called NO-NO_2-O_3 triad are constant with height within the atmospheric surface layer. This implies that the trace compounds are considered chemically non-reactive tracers (Trebs et al., 2006). However, if characteristic chemical time scales (τ_{chem}) of trace substances, such as NO_2, are shorter than the corresponding time scales of turbulent transport, this prerequisite is not met. The Damköhler theory has been introduced to evaluate whether or not chemical reactions violate the "constant flux layer assumption" (De Arellano and Duynkerke, 1992). In order to estimate τ_{chem} for the NO-NO_2-O_3 triad, $j(NO_2)$ must be known (Lenschow, 1982). Moreover, a simple tool to evaluate the photochemical steady state (PSS) assumption of NO_x (Leighton, 1961) in the absence of $j(NO_2)$ measurements is required, especially for examining the local peroxy radical photochemistry and the photochemical ozone tendency (e.g., Yang et al., 2004; Mannschreck et al., 2004).

Direct measurements of $j(NO_2)$ at ground level using spectroradiometers (SR) or filter radiometers (FR) are often not available from field experiments (e.g., during NitroEurope-IP, Sutton et al., 2007). Although several approaches exist to estimate $j(NO_2)$, most of them involve complex radiative transfer algorithms that depend on the knowledge of local atmospheric parameters such as aerosol optical thickness (AOT), ozone column and cloud cover (Cotte et al., 1997; Madronich, 1987b; Ruggaber et al., 1993; Wiegand and Bofinger, 2000). Some studies also use parameterizations only including SZA to calculate $j(NO_2)$ at ground level, which, however, is limited to clear-sky conditions (Dickerson et al., 1982; Parrish et al., 1983). For many sites this approach is rarely applicable, since high loadings of aerosols as well as clouds strongly influence $j(NO_2)$ (e.g., Monks et al., 2004; Thielmann et al., 2001).

Compared to $j(NO_2)$, measurements of the solar global irradiance (G) are more common because this quantity constitutes a fundamental meteorological parameter: the total solar radiant flux density incident on a flat surface. While cloud observations by monitoring stations worldwide have decreased in the last decades, several surface radiation monitoring networks have been established (e.g., Baseline Surface Radiation Network, FLUXNET, World Radiation Data Centre as part of the WMO Global Atmospheric Watch Program) where G is measured as a standard parameter. G is also often measured as part of automated weather stations using pyranometers, which determine the total of direct plus diffuse solar irradiance between 300 nm and 3000 nm. The horizontal surface of the G sensor produces a cosine response to the directions of the incoming radiation due to the reduced projected area of the surface for SZAs other than 0° (e.g., Zafonte et al., 1977). In contrast, the actinic flux is the unweighted radiance integrated over a sphere. Although there is a difference in the receiver geometry and also in the wavelength range for the reception of irradiance and actinic flux, near-linear relationships between $j(NO_2)$ and G were proposed (Bahe et al., 1980; Brauers and Hofzumahaus, 1992; Schere and Demerjian, 1978; Wratt et al., 1992). In other studies, a curvature in the relation between UV-A actinic flux and irradiance was found (e.g., Madronich, 1987a; van Weele et al., 1995; Zafonte et al., 1977). McKenzie et al. (2002) and van Weele et al. (1995) suggested that $j(NO_2)$ may be estimated from measurements of G or spectral irradiances within an accuracy of 20%. In this study, we propose an empirical second-order polynomial function that can be used to estimate $j(NO_2)$ solely from G. In contrast to previous studies, our results also include solar zenith angles smaller than 30° and are based on field observations in temperate, subtropical and tropical environments.

2 Experimental

2.1 Site descriptions

Table 1 provides an overview of the field sites and the sensors used for the radiation measurements. All of the measurements in Table 1 were obtained from ground-based stations under various environmental conditions (e.g., Earth-Sun distance, urban versus rural environments, elevation above sea level, cloud and haze conditions, overhead O_3 column, and regional surface albedo, cf. Madronich, 1987a).

2.1.1 Site 1: Marondera (Zimbabwe)

Measurements were performed at the Grasslands Research Station, Marondera, Zimbabwe. The site is located 8 km west of Marondera and about 60 km south-east of Harare

Table 1. Overview of the field sites and the sensors used for the radiation measurements. UV-A surface albedo ranges were estimated using results from Feister and Grewe (1995).

site	Marondera Central Zimbabwean Plateau Zimbabwe (site 1)	Jarú Amazon Basin Rondônia Brazil (site 2)	Jülich Research Center Germany (site 3)	Hohenpeißenberg Bavaria Germany (site 4)	Jungfraujoch High Altitude Research Station Switzerland (site 5)
measurement periods	10 Oct–1 Dec 1994	19–21 May 1999 20–24 Oct 1999	16 Jun–29 Jul 2002	7–20 Sep 2005	22 Jul–29 Aug 2001 8 Mar–17 Apr 2002 7 Apr–10 May 2005
campaign	–	LBA-EUSTACH	ECHO	SALSA	–
Lat/ Lon	18°11′ S/ 31°28′ E	10°05′ S/ 61°56′ W	50°54′ N/ 6°25′ E	47°47′ N/ 10°59′ E	46°33′ N/ 7° 59′ E
elevation (a.s.l.)	1630 m	147 m	91 m	735 m	3580 m
vegetation/site	savanna	rain forest	decidous forest/ building	grassland	none (Research station)
UV-A albedo range	0.05–0.2	0.02–0.05	0.02–0.1	0.02	0.1–0.8
climate	subtropical	tropical	temperate	temperate	temperate
measurement height (a.g.l.)	1 m ($j(NO_2)$) 2 m (G)	51.7 m	15 m ($j(NO_2)$) 10 m (G)	2 m	200–2000 m
$j(NO_2)$ sensor	filter radiometer	filter radiometer	spectro-radiometer	filter radiometer	spectro-radiometer
G sensor	pyranometer LI-200SZ, (LI-COR)	pyranometer LI-200SZ, (LI-COR)	pyranometer CM 7 (Kipp & Zonen B.V.)	pyranometer CM21 (Kipp & Zonen B.V.)	Eppley Pyranometer (Modell PSP)
reference	Meixner et al. (1997)	Andreae et al. (2002)	Bohn (2006)	Acker et al. (2006)	Fluckiger (2002)

site	Guangzhou Backgarden Pearl River Delta China (site 6)	Oensingen Central Swiss Plateau Switzerland (site 7)	Fichtelgebirge Bavaria Germany (site 8)	Mainz Max Planck Institute for Chemistry Germany (site 9)
measurement periods	30 Jun–29 Jul 2006	21 Jul–5 Sep 2006	7–30 Sep 2007	25 Jan–25 Feb 2008
campaign	Pearl River Delta Campaign	NitroEurope	EGER	–
Lat/ Lon	23°29′ N/ 113°02′ E	47°17′ N/ 7°44′ E	50°09′ N/ 11°52′ E	49°59′ N/ 8°14′ E
elevation (a.s.l.)	13 m	450 m	775 m	131 m
vegetation/site	grassland/ building	grassland	spruce forest	none (roof of building)
UV-A albedo range	0.02–0.1	0.02	0.02–0.05	0.1
climate	tropical/subtropical	temperate	temperate	temperate
measurement height (a.g.l.)	11 m ($j(NO_2)$) 1 m (G)	1.5 m ($j(NO_2)$) 3 m (G)	28 m ($j(NO_2)$) 30 m (G)	25 m
$j(NO_2)$ sensor	spectro-radiometer	filter radiometer	filter radiometer	filter radiometer
G sensor	BT-1 (Chinese Academy of Meteorological Science)	pyranometer CM3 (Kipp & Zonen B.V.)	pyranometer CM14 (Kipp & Zonen B.V.)	pyranometer LI-200SZ, (LI-COR)
reference	Garland et al. (2008)	Ammann et al. (2007)	Gockede et al. (2007)	–

on the central Zimbabwean plateau (Meixner et al., 1997). This region falls within the so-called broad-leaved savanna, although the vegetation was almost completely withered during our measurements at the end of the dry season. The local climate is characterized by a long dry season (8 months) and a short wet/rainy season. Mean monthly temperatures range from 11.7°C (June) to 19.0°C (November), and more than 80% of the mean annual rainfall (846 mm) occurs between November and March (Meixner et al., 1997).

2.1.2 Site 2: Jarú (Brazil)

Measurements were done within the framework of the LBA-EUSTACH project (EUropean Studies on Trace gases and Atmospheric CHemistry as a contribution to Large-scale Biosphere-atmosphere experiment in Amazonia, Andreae et al., 2002). The experimental site was located in the Reserva Biológica Jarú, a forest reserve 90 km north of the city of Ji-Paraná in the state of Rondônia (Amazon Basin, Brazil). Our radiation measurements were performed at the end of the wet season (clean background conditions) from 19–21 May 1999, and at the end of the dry season, which is characterized by strong biomass burning activities, from 20–24 October 1999. The site is characterized by a humid tropical climate (Culf et al., 1996; Gash and Nobre, 1997) with a mean annual rainfall of about 2500 mm and a mean annual temperature of about 26°C. In 1999, the vegetation cover at the Jarú site consisted of primary (terra firme) open rain forest with a closed canopy of about 32 m height (Rummel et al., 2002; Rummel et al., 2007).

2.1.3 Site 3: Jülich (Germany)

Measurements were performed within the framework of the ECHO 2002 campaign (Emission and chemical transformation of biogenic volatile organic compounds: Investigations in and above a mixed forest stand) on top of a building close to the main forest measurement site (Bohn, 2006). The region is dominated by agriculture and forests. The climate is temperate with an average annual rainfall of 685 mm and a mean annual temperature of 9.7°C.

2.1.4 Site 4: Hohenpeißenberg (Germany)

The experimental site was a managed and fertilized meadow located at the WSW-slope of the mountain Hoher Peißenberg (summit 988 m a.s.l., Hohenpeißenberg Meteorological Observatory of the German Weather Service), directly west of the village Hohenpeißenberg in Bavaria, Southern Germany (Winkler, 2006). The surrounding pre-alpine landscape is characterized by its glacially shaped, hilly relief and a patchy land use dominated by the alternation of cattle pastures, meadows, mainly coniferous forests and rural settlements. The climate is temperate, with a mean annual temperature of 6.4°C (record from 1781–2008) and an average annual precipitation of 1129 mm.

2.1.5 Site 5: Jungfraujoch (Switzerland)

Measurements were made at the Sphinx observatory that is located on a crest in the Bernese Alps between the mountains Jungfrau and Mönch at 3580 m altitude (cf. Fluckiger, 2002). Towards South-East the surrounding is mainly snow and ice covered rocks with glaciers, whereas towards North-West the Swiss midlands are usually snow-free, as they are more than 2000 m below the station. The average temperature is about −8°C.

2.1.6 Site 6: Guangzhou (China)

The radiation measurements at Guangzhou (capital city of Guangdong Province) were performed within the framework of the PRIDE-PRD2006 (*P*rogram of *R*egional *I*ntegrate*d* *E*xperiments on Air Quality over *P*earl *R*iver *D*elta of China 2006) Campaign. Measurements were made at the site in Backgarden, a small village in a rural farming environment on the outskirts of the densely populated center of the PRD situated about 48 km northwest of Guangzhou (cf. Garland et al., 2008; Hofzumahaus et al., 2009). The $j(NO_2)$ sensor was installed on the top of a 10 m high hotel building, while the G sensor was located at a nearby grassland site. The climate is tropical to subtropical; the mean annual precipitation is about 1500–2000 mm with a mean annual temperature of ∼19°C.

2.1.7 Site 7: Oensingen (Switzerland)

The experimental site was located on the Central Swiss Plateau near the village of Oensingen in the north-western part of Switzerland. The region is characterized by a relatively small scale pattern of agricultural fields (grassland and arable crops). The measurement field is covered by a grass-clover mixture. The climate is temperate with an average annual rainfall of about 1100 mm and a mean annual temperature of 9.5°C (Ammann et al., 2007).

2.1.8 Site 8: Fichtelgebirge (Germany)

The site was located in the Fichtelgebirge mountains in Northeastern Bavaria. The arched, densely forested Fichtelgebirge (ca. 1000 km^2) lies in the northeastern part of Bavaria (district of Oberfranken; near the frontier to the Czech Republic). Measurements were done on a meteorological tower surrounded by hilly terrain with slopes of moderate steepness. The area is mainly covered by spruce forest with a mean canopy height of 23 m around the tower. The climate is temperate with an average annual rainfall of about 1200 mm and a mean annual temperature of 5.3°C.

2.1.9 Site 9: Mainz (Germany)

Measurements were conducted on the roof of the Max Planck Institute for Chemistry in Mainz, which is located at the western margin of the urban agglomeration of the

Rhein-Main area. The climate is temperate with an average annual rainfall of about 585 mm and a mean annual temperature of 9.6°C.

2.2 Solar global irradiance measurements

The pyranometer sensors employed at sites 3, 4, 7, and 8 (see Table 1) were manufactured by Kipp & Zonen. They measure the total solar irradiance and have an accuracy of ±3%. The CM series from Kipp & Zonen provide a flat spectral response for the full solar spectrum range. The other type of pyranometer sensor, used for the measurements at sites 1, 2 and 9 (see Table 1), is manufactured by LI-COR and has an accuracy of ±5%. The spectral sensitivity of this sensor is less broad than that of the CM series from Kipp & Zonen and is also not constant over the solar spectrum. We have intercompared the Kipp & Zonen (CM14) and the LI-200SZ pyranometer sensor, e.g., at the Jarú rainforest site in Brazil 1999. The slope of the linear regression was ∼0.99 and r^2 was ∼0.99. Obviously, the different characteristics and spectral sensitivities of the global radiation sensors did not significantly influence the results. At the Jungfraujoch (site 5), an Eppley Pyranometer (Modell PSP) was used, which is a World Meteorological Organization First Class Radiometer with an accuracy of ±4%. In Guangzhou (site 6), a BT-1 global radiation sensor was used (accuracy ±5%), manufactured by the Institute of Atmospheric Sounding, Chinese Academy of Meteorological Science.

Additionally, sunshine duration was measured using a photoelectric (SONI e3, Siggelkow, Germany) and a Campbell-Stokes sunshine recorder (Lamprecht, Germany) in Jülich and Hohenpeißenberg, respectively.

2.3 $j(NO_2)$ measurements

The spectral actinic flux was measured either integrated over a suitable wavelength range by $j(NO_2)$-filter radiometers, or spectrally resolved by spectroradiometers covering the whole UV range. Bohn et al. (2008) demonstrated that $j(NO_2)$-filter radiometers are reliable instruments for $j(NO_2)$ measurements, with excellent linearity, low detection limits and long-term stability of calibration factors. The filter radiometers employed in this study at Marondera, Jarú, Hohenpeißenberg, Oensingen, Fichtelgebirge and Mainz (sites 1, 2, 4, and 7–9, see Table 1) are of the same type as examined by Bohn et al. (2008) (Meteorologie Consult GmbH, Königstein, Germany). Their setup and principle of operation follow that described by Volz-Thomas et al. (1996). The filter radiometer employed during the 1994 and 1999 campaigns (Marondera and Jarú, sites 1 and 2) was calibrated before the field experiments against a master $j(NO_2)$ radiometer by the manufacturer. The master radiometer was compared against the former chemical actinometric system at Forschungszentrum Jülich. Calibrations of the filter radiometers during the field campaigns Hohenpeißenberg, Oensingen, Fichtelgebirge and Mainz (sites 4 and 7–9) were made prior and/or after the installation of the instruments at the field sites using a spectroradiometer with absolute spectral calibration as a reference (Hofzumahaus et al., 1999). The spectral calibration is traceable to a primary irradiance standard (blackbody BB3200pg of the Physikalisch-Technische Bundesanstalt, PTB). For the calculation of $j(NO_2)$ from the actinic flux spectra, the absorption cross section and quantum yield data of Merienne et al. (1995) and Troe (2000) were used. These molecular data were selected because they gave consistent results within 5–10% in comparisons with chemical actinometer measurements of $j(NO_2)$ (Kraus et al., 2000; Shetter et al., 2003). The same molecular data were used in the analysis of the data obtained at Jülich and Guangzhou (sites 3 and 6, Table 1), where double monochromator and single monochromator based spectroradiometers were employed, respectively. Spectroradiometer and filter radiometer measurements of $j(NO_2)$ are therefore based on the same molecular data of NO_2. More information on the spectroradiometer instruments is given elsewhere (Bohn et al., 2008).

The $j(NO_2)$ measurements at Jungfraujoch (site 5) were also made with a spectroradiometer. The spectroradiometer was regularly calibrated against a 1000 W standard lamp, traceable to PTB. Photolysis frequencies were initially calculated according to the NASA-JPL recommendation of 1997 (DeMore et al., 1997). These recommendations resulted in $j(NO_2)$ values that were 10.5% lower compared to the use of cross-sections from Merienne et al. (1995) and quantum yields from Troe (2000), virtually independent of external conditions. Thus, the Jungfraujoch data were scaled accordingly. The overall accuracy of the radiometric $j(NO_2)$ measurements using spectroradiometers or calibrated filter radiometers was estimated to 10% (Bohn et al., 2008).

The $j(NO_2)$ and G values measured at each site were synchronized to half-hourly averages. Outliers were identified and removed manually due to repeated occurrence at the same time of the day potentially caused by temporary shadowing effects from adjacent objects, e.g., masts. The number of outliers in the data sets was less than 1% of the total number of data points.

3 Results

In principle, $j(NO_2)$ results from the integral UV radiation from all directions. However, like for the total shortwave radiation, the contribution from the lower hemisphere (reflected by the surface) is generally much smaller than from the upper hemisphere. Thus in many field experiments, only the downwelling (upper hemisphere 2π sr) contribution to $j(NO_2)$ was measured (henceforth abbreviated as $j(NO_2)\downarrow$). Regarding $j(NO_2)\uparrow$ refer to Sect. 4.6.

We plotted the half-hourly averaged $j(NO_2)\downarrow$ values versus respective G values observed for all nine measurement sites (Fig. 1). Although a wide range of atmospheric conditions was covered by the measurements, the results

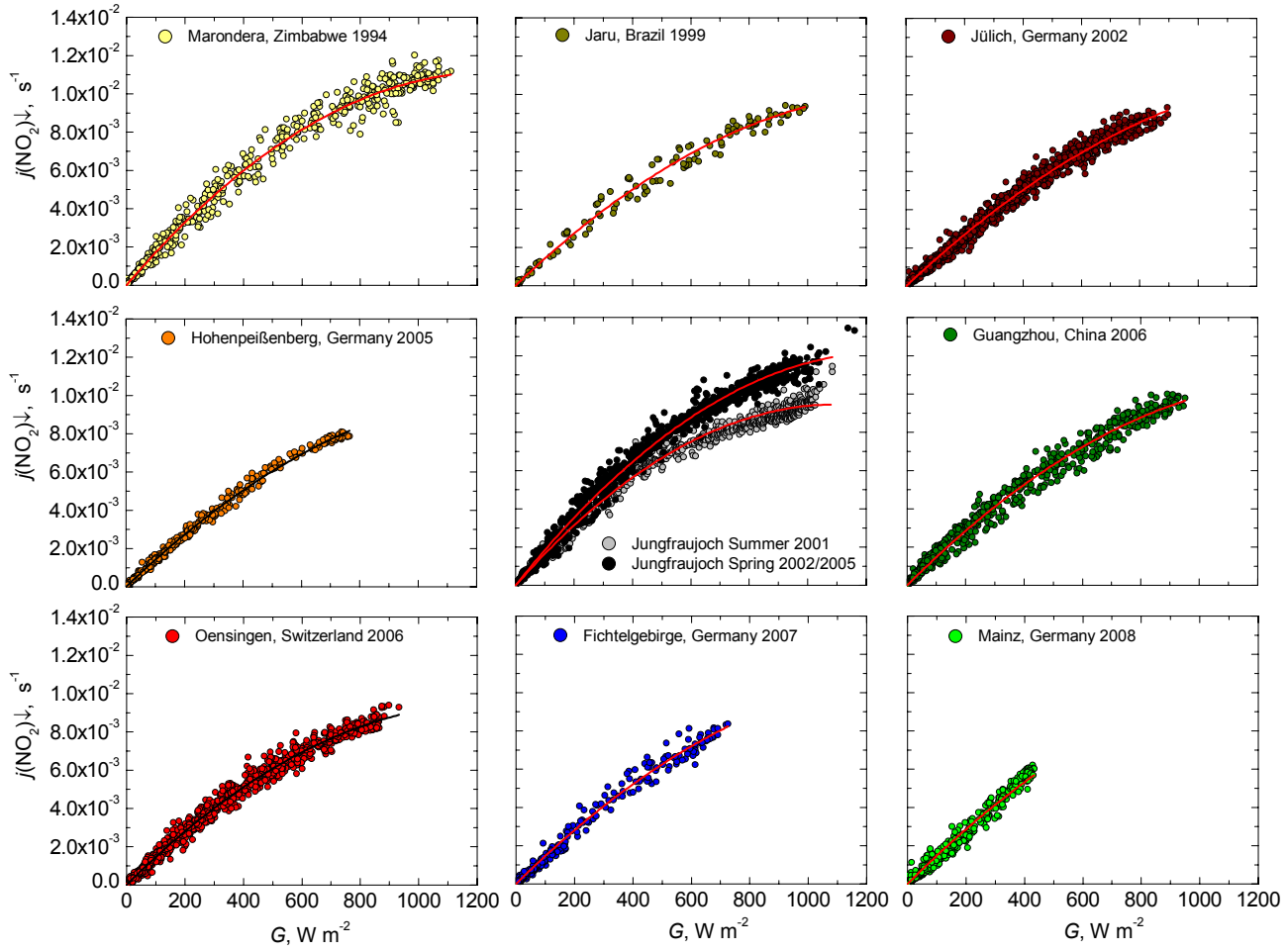

Fig. 1. Scatter plots of $j(NO_2)\downarrow$ vs. G (half-hourly averages) measured at the nine field sites listed in Table 1 (including cloudy and clear-sky conditions) and corresponding unweighted second-order polynomial fit curves (for details see Table 2).

Table 2. Results for unweighted polynomial curve fitting $j(NO_2)\downarrow = B_1 \times G + B_2 \times G^2$ (with $j(NO_2)$ intercept = 0) of the measured downwelling NO_2 photolysis frequency versus solar global irradiance for all sites (data for cloudy and clear-sky conditions were used for curve fitting, for details see text).

site	Marondera	Jarú	Jülich	Hohen-peißenberg	Jungfraujoch		Guangzhou	Oensingen	Fichtel-gebirge	Mainz
	Zimbabwe	Brazil	Germany	Germany	Switzerland		China	Switzerland	Germany	Germany
	(site 1) 1994	(site 2) 1999	(site 3) 2002	(site 4) 2005	(site 5) 2001 (summer)	2002/2005 (spring)	(site 6) 2006	(site 7) 2006	(site 8) 2007	(site 9) 2008
Number of data points (N)	681	125	1366	495	848	539	684	1294	342	509
B_1, $W^{-1}\,m^2\,s^{-1}$	1.78×10^{-5}	1.47×10^{-5}	1.44×10^{-5}	1.47×10^{-5}	1.72×10^{-5}	1.91×10^{-5}	1.53×10^{-5}	1.52×10^{-5}	1.51×10^{-5}	1.53×10^{-5}
B_2, $W^{-2}\,m^4\,s^{-1}$	-7.11×10^{-9}	-5.32×10^{-9}	-4.62×10^{-9}	-5.26×10^{-9}	-7.82×10^{-9}	-7.47×10^{-9}	-5.42×10^{-9}	-6.08×10^{-9}	-5.18×10^{-9}	-5.00×10^{-9}

generally show a compact, non-linear dependence between $j(NO_2)\downarrow$ and G. While the lower part of the graphs up to a value of $G \approx 450\,W\,m^{-2}$ appears to be linear, the overall relationship shows a clear curvature with reduced slopes in the high G range. Most measurements were made during the summer, except those at Mainz (Germany), which were made during winter and show a near-linear dependency ($G < 450\,W\,m^{-2}$).

As a first approach, Table 2 presents results from second-order polynomial curve fittings of the data for the different sites according to:

$$j(NO_2)\downarrow = B_1 \times G + B_2 \times G^2 \quad (1)$$

The coefficients B_1 and B_2 were obtained by an unweighted Levenberg-Marquardt least-squares minimization. The polynomials were forced through the origin, because co-fitted intercepts B_0 were always close to zero and both quantities are zero at night. The coefficients B_1 and B_2 are very similar for most sites, except for those which are located higher than 800 m a.s.l. (Marondera and Jungfraujoch). Because of the good agreement of the relationships between $j(NO_2)\downarrow$ and G for all sites below 800 m a.s.l., we pooled the respective data for further analysis. These data are shown in Fig. 2a, where a consistent, site-independent behavior is evident. For comparison, a previously proposed linear relation by Bahe et al. (1980) was included, which differs by up to 50%, depending on G.

A prerequisite for accurate fitting of the parameters B_1 and B_2 to the data in Fig. 2a is an adequate weighting of data points with random and/or systematic measurement errors. These may consist of, e.g., radiometric measurement uncertainties and calibration errors, respectively. However, these errors are hard to estimate and cannot be assigned to either $j(NO_2)\downarrow$ or G values, because our data scatter is partly caused by synchronization problems of the different measurements. To account for the varying density of data points and their scatter, we binned the $j(NO_2)\downarrow$ data into 10 W m^{-2} – G intervals and calculated mean $j(NO_2)\downarrow$ values and the corresponding standard deviations. These data are plotted in Fig. 2b. We then made a least-squares minimization where the data points were weighted with the $j(NO_2)\downarrow$ standard deviations. The resulting polynomial coefficients B_1 and B_2 were determined to: $B_1 = (1.47 \pm 0.03) \times 10^{-5}$ W^{-1} m^2 s^{-1} and $B_2 = (-4.84 \pm 0.31) \times 10^{-9}$ W^{-2} m^4 s^{-1}. It should be noted that the parameters B_1 and B_2 are highly correlated and that the relationship in Eq. (1) is empirical, i.e., there is no obvious physical reason why a second-order polynomial fit is appropriate. However, Fig. 3a shows that the $j(NO_2)\downarrow$ residuals are nearly normally distributed. Figure 3b shows the absolute $j(NO_2)\downarrow$ residuals versus G along with the $\pm 2\sigma$ (95.45%) confidence band of $\pm 6 \times 10^{-4}$ s^{-1}. The $j(NO_2)$ residuals vary randomly around zero and the spread of the residuals is about the same throughout the plot, indicating that the $j(NO_2)\downarrow$ residual variance exhibits no dependence on G, which justifies our fitting approach. Figure 3c illustrates a substantial decrease of the relative $j(NO_2)\downarrow$ residual towards higher G values. For $G < 100$ W m^{-2} the relative deviation of the measured values (half-hourly averages) from the fitted function is often considerably higher than 40%. For G between 100 and 500 W m^{-2} the relative deviation of the measured values from the fitted function ranges from 10 to 40% and for $G > 500$ W m^{-2} the deviation is lower than 10% (2σ). Since

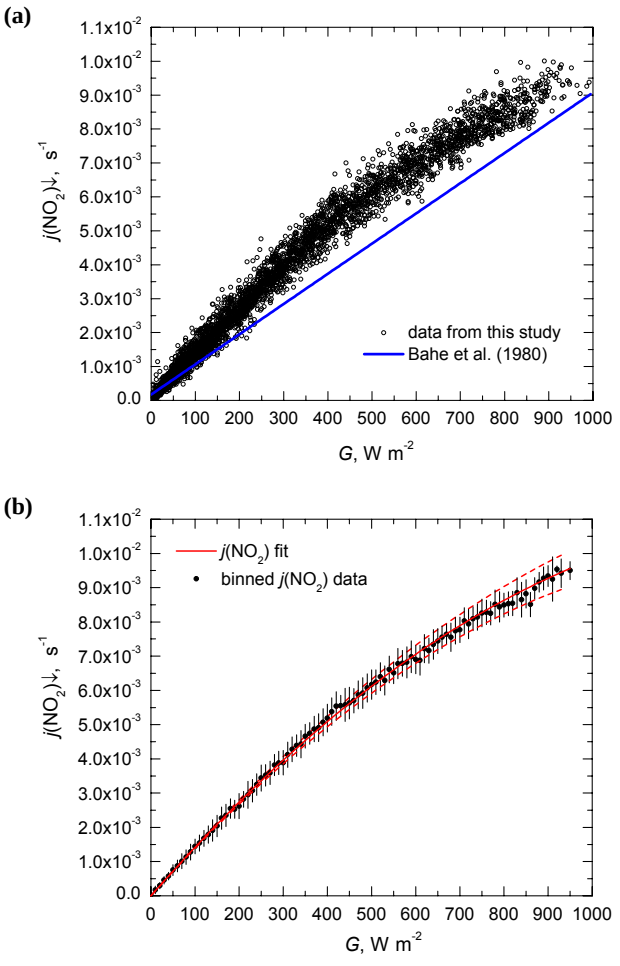

Fig. 2. **(a)** Scatter plot of $j(NO_2)\downarrow$ vs. G (half-hourly averages) for all data from sites located below 800 m a.s.l. (cloudy and clear-sky conditions are included, N=4815). For comparison, a previously published linear parameterization is also displayed. **(b)** Mean $j(NO_2)\downarrow$ values (black filled circles) and corresponding standard deviations (error bars) versus 10 W m^{-2} – G intervals (N=95) with weighted second-order polynomial fit (red line, r^2=0.99), uncertainty range of the fitted function calculated from the errors of B_1 and B_2 is shown as red dashed lines. For further explanations see text.

the distribution of relative residuals of individual sites was comparable to that in Fig. 3c, we did not find an indication that measurements at one or more sites deviated systematically from the overall fitted relationship. For test purposes we also binned the G data into 10^{-4} s^{-1} – $j(NO_2)\downarrow$ intervals and fitted the reverse function to obtain the parameters B_1 and B_2. The obtained parameters were similar within their error limits, namely $B_1 = (1.44 \pm 0.02) \times 10^{-5}$ W^{-1} m^2 s^{-1}, $B_2 = (-4.24 \pm 0.29) \times 10^{-9}$ W^{-2} m^4 s^{-1}. The corresponding parameterisation is hard to distinguish from that shown in Fig. 2b.

In order to check whether the empirically found relationship between $j(NO_2)\downarrow$ and G can be reproduced by

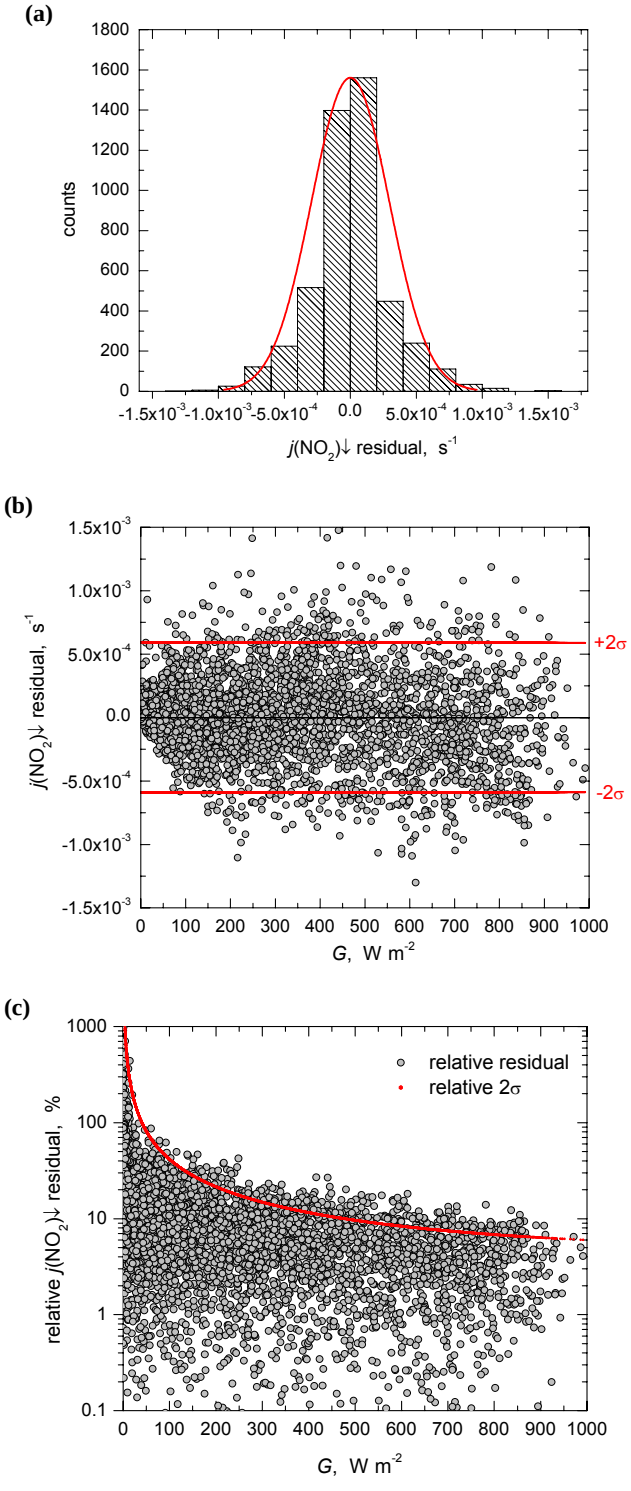

Fig. 3. Residual analysis for polynomial fit shown in Fig. 2b including **(a)** histogram of the $j(NO_2)\downarrow$ residuals with Gaussian probability distribution (red line) **(b)** plot of absolute $j(NO_2)\downarrow$ residuals versus G with $\pm 2\sigma$ confidence bands (red lines) and **(c)** relative $j(NO_2)\downarrow$ residual versus G with relative 2σ confidence band (red line).

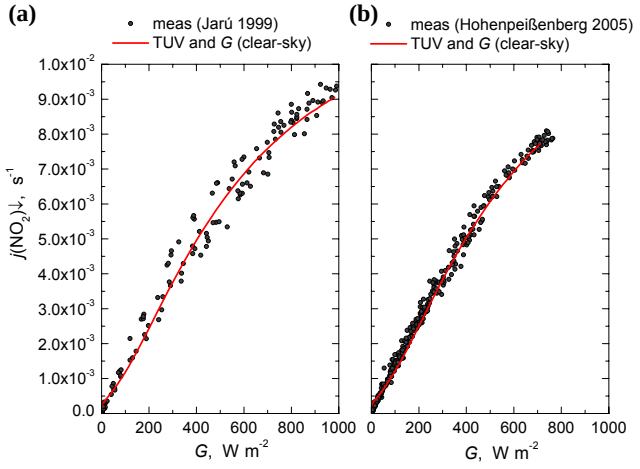

Fig. 4. Clear-sky $j(NO_2)\downarrow$ for a simple model atmosphere predicted with the Tropospheric Ultraviolet Visible (TUV) model (http://cprm.acd.ucar.edu/Models/TUV/) versus G from a parameterization of Paltridge and Platt (1976) exemplarily for **(a)** 21 May 1999 at the Jarú site in Brazil (site 2) and **(b)** 9 September 2005 at the Hohenpeißenberg site in Germany (site 4). The parameterization from Paltridge and Platt (1976) is based on measurements in Australia and was scaled by a factor of 0.9 to match the experimental data of this study. Partly, this discrepancy can be explained by the lower Sun-Earth distance during the southern hemisphere summer season.

theoretical calculations, we applied a radiative transfer model, using sites 2 and 4 as examples. The Tropospheric Ultraviolet Visible (TUV) model (http://cprm.acd.ucar.edu/Models/TUV/) (version 4.4) was used to calculate clear-sky $j(NO_2)\downarrow$ for a simple model atmosphere. The molecular data used in the TUV model were consistent with those used above (Merienne et al., 1995; Troe, 2000). The model was set up with the following parameters: UV-A surface albedo $\alpha = 0.03$ (cf. Feister and Grewe, 1995), O_3 column = 300 DU, NO_2 column = 0.3 DU, no clouds, AOT (550 nm) = 0.235 (scaled to different wavelengths using an Angstrom exponent of 1.0), single scattering albedo $\omega_0 = 0.99$. Since our measurements of G include wavelengths of up to 3000 nm and the TUV model code stops at 1000 nm, we used a parameterization by Paltridge and Platt (1976) to estimate potential clear-sky G (Niemela et al., 2001). The predicted clear-sky $j(NO_2)\downarrow$ is plotted versus estimated clear-sky G for the two selected sites in Fig. 4a and b. It shows that the model results reproduce the overall relationship relatively well, although the clear sky parameterization of G represents a rather crude approximation using only the SZA as input. More complex and accurate formulas were derived in the literature (Niemela et al., 2001) but an assessment of these formulas is beyond the scope of this study. A near linear relationship between $j(NO_2)$ and G under clear-sky conditions below about 400 W m^{-2} was also reproduced qualitatively using TUV simulations at wavelengths below 1000 nm. The linearity turned out to be accidental because

diffuse and direct contributions to $j(NO_2)$ rise oppositely at low G (parabolic for direct and hyperbolic for diffuse radiation).

4 Discussion

4.1 Shape of the relationship between $j(NO_2)\downarrow$ and G

In Sect. 3 we have established an empirical relationship between the irradiance integrated over the short-wave solar spectrum and the downwelling photolysis frequency $j(NO_2)\downarrow$, a quantity that is proportional to the upper hemispheric UV-A actinic flux. The fundamental difference between irradiance and actinic flux is that irradiance is describing a photon (or energy) flux density on a unit horizontal surface by weighting the radiance with the cosine of the SZA upon integration over the solid angle field of view (e.g., Schallhart et al., 2004; Webb, 2003; Webb et al., 2002a). For example van Weele et al. (1995) and Webb et al. (2002b) have shown that the ratio of actinic flux and the downward irradiance depends on α, SZA and the ratio of direct to total downward irradiance and also on the amount and isotropy of scattering in the atmosphere. The curvature of the relationships plotted in Figs. 1 and 2a, b increases with decreasing SZAs (increasing G), when the proportion of direct radiation becomes larger because of the lower atmospheric scattering at small SZAs. Generally, the actinic flux varies more slowly in time than the spectral irradiance (see also Kazadzis et al., 2000; Kylling et al., 2003; McKenzie et al., 2002; Webb et al., 2002b). This implies that the curvature in Figs. 1 and 2a, b represents an almost vanishing $j(NO_2)\downarrow$ increase at small SZAs, while G is still benefiting from the increase of the cosine weighting factor. Correlating $j(NO_2)$ with the UV irradiance also results in a curvature with increasingly higher values of the UV irradiance (Madronich, 1987a) and consistently, the relationship between UV-A irradiance and G can be described by a near-linear dependency (Canada et al., 2003; Jacovides et al., 2006; Kudish and Evseev, 2000; Ogunjobi and Kim, 2004).

However, some previous studies also found near-linear relationships between $j(NO_2)$ and G (e.g., Bahe et al., 1980; Brauers and Hofzumahaus, 1992; Schere and Demerjian, 1978; Wratt et al., 1992). Brauers and Hofzumahaus (1992) made a linear fit though their data collected over the Atlantic, although a curvature was evident from their plot. Bahe et al's measurements in Bonn, Germany (70 m a.s.l.) did not include SZAs smaller than 30° and a substantial data scatter was observed. Although Bahe et al's measurements covered periods of dawn and sunset until darkness; they state that their linear function contains an intercept that has no physical significance (cf. Fig. 2a). It should be noted that the model predictions in Fig. 4a and b also reveal an intercept (i.e., $j(NO_2)\downarrow > 0$ at clear-sky $G{=}0$) that is even slightly higher than the one determined by Bahe et al. (1980). This can be explained by several effects. First, the G-parameterization is forced through zero at SZA = 90° and therefore does not allow for twilight. Second, because of the refraction of the atmosphere, the actual sunset is delayed and the sunrise is premature, which is not considered in the calculations. Third, the pseudo-spherical correction of TUV for atmospheric curvature may overestimate $j(NO_2)\downarrow$ at SZA approaching 90°. Our measurements did not suggest a significant intercept between the relationship of $j(NO_2)\downarrow$ and G, but it should be kept in mind that in particular the G measurements approach the limit of detection at dawn and sunset.

Reuder (1999) has also shown previously for four sites in Germany and France that the relationship between $j(NO_2)\downarrow$ and G can be described by a second-order polynomial function with a $j(NO_2)\downarrow$ intercept = 0. He found similar coefficients B_1 and B_2 as presented in Table 2. Madronich (1987a) argued that expressing $j(NO_2)$ as a polynomial function of the irradiance may only work for individual days, but the seasonal variation of $j(NO_2)$ cannot be reproduced accurately. The reason is the variation of the Sun-Earth distance affecting $j(NO_2)$ and G differently, because of the cosine weighting included in G. However, we consider this a minor effect that is not evident in our data within experimental errors and variations caused by atmospheric effects, e.g., clouds. The main atmospheric factors affecting G and $j(NO_2)$ will be discussed in more detail in the following sections.

4.2 Water vapour

The solar short-wave irradiance incident at ground level depends on the atmospheric water vapour column. On the other hand, there is no direct influence of water absorption on $j(NO_2)$. The relation between $j(NO_2)$ and G is therefore expected to depend on atmospheric water concentrations. Direct measurements of water columns are not available for the different measurement sites. Ground based measurements of relative humidity exist but these are only representative for the boundary layer and cannot be converted accurately to total atmospheric water columns. However, at least for model atmospheres, there is a correlation between water vapour concentration at the ground and total water columns (Tomasi et al., 1998). This relation was used to estimate the water columns at the sites Guangzhou and Jülich. The results are consistent with satellite data (e.g., MODIS), which indicate typical ranges of about 1–4 cm of precipitable water for Europe and 4–7 cm for the tropics. However, no water dependence was evident in the $j(NO_2) - G$ correlations for the estimated ranges (4–6 cm for Guangzhou, 1.5–4.5 cm for Jülich). The reason for the missing evidence is probably the strong non-linearity of the attenuation of solar irradiance by water vapour and the fact that extremely dry conditions were not encountered. At normal incidence, water columns of 1 cm and 10 cm lead to attenuations of about 150 $W\,m^{-2}$ and 250 $W\,m^{-2}$, respectively (Houghton, 1986). Thus, the natural variability of water vapour is expected to influence the data in Fig. 2, but overall the scatter is probably dominated by

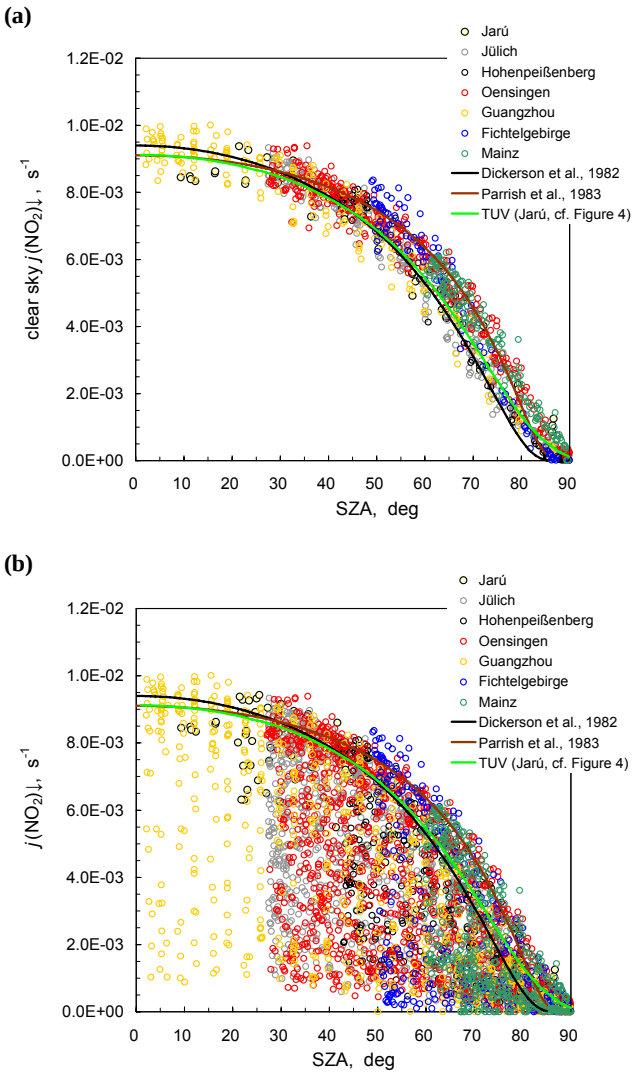

Fig. 5. Plots of $j(NO_2)\downarrow$ versus SZA **(a)** under clear-sky and **(b)** under clear-sky and cloudy conditions for seven field sites below 800 m a.s.l. The empirical functions of Dickerson et al. (1982) and Parrish et al. (1983) are also shown, as well as results from the TUV model exemplarily for the Jarú site.

other effects, most importantly by clouds. However, stronger deviations from our empirical relationship cannot be ruled out for extremely low water concentrations (e.g., polar regions), which were not covered by our measurements.

4.3 Clouds

Blumthaler et al. (1994) and Dickerson et al. (1982) state that clouds attenuate total solar irradiance by about 20% more than UV irradiance in the region of NO_2 photolysis. Moreover, UV irradiance and $j(NO_2)$ are not attenuated by clouds in the same manner (Parrish et al., 1983). In Fig. 5a and b we plotted measured $j(NO_2)\downarrow$ versus SZA under clear sky and all conditions, respectively. For comparison, also the empirical functions of Dickerson et al. (1982) and Parrish et al. (1983) that only use the SZA to calculate $j(NO_2)$ were included, as well as the TUV modeled data (exemplarily for the Jarú site, cf. Fig. 4a). Under clear-sky conditions the empirical functions fit relatively well to our experimental values for SZA $< 70°$, but obviously they cannot be used to predict $j(NO_2)$ for cloudy conditions. The same applies for the TUV and other radiation transfer calculations unless detailed information about cloud properties is available. However, despite this pronounced effect of clouds, conditions with and without clouds cannot be distinguished in Fig. 2. Under overcast conditions, i.e. in the absence of direct sun, a linear relationship between G and $j(NO_2)$ is expected but G will remain below about 400 W m^{-2}. The actual slope depends on the distribution of sky radiance and the fraction of UV-A and shortwave radiation absorbed by the clouds, but within experimental error the typical slope appears to be similar to that under clear sky conditions. This similarity is considered accidental and cannot be rationalized by simple assumptions.

Broken cloud conditions with occasional sunshine and reflections at cloud sides are expected to induce significant deviations from the simple relationship in Fig. 2. However, these deviations are usually temporary and widely eliminated by the 30 min averaging periods. A data set with higher time resolution (not considered in this work) indeed shows increased scatter, which gradually decreases upon extending the averaging period but a quantitative assessment of these short term fluctuations is not feasible based on the available information.

The general validity of the empirical relationship in Fig. 2 under all conditions is confirmed in Fig. 6a and b, where the data from Jülich and Hohenpeissenberg were plotted and classified using the locally measured sunshine duration as a proxy for the cloud cover. Except for the fact that the largest values of $j(NO_2)$ and G were only obtained for periods with high sunshine duration (as expected) there is no apparent further dependence on this quantity.

4.4 Aerosol load

The atmospheric aerosol load is expected to have spectrally different effects on G and $j(NO_2)\downarrow$ at different locations, depending on the prevailing type of aerosols (soot, sulfate, organics, dust, etc.). The AOT provides quantitative information about the extinction of solar radiation by aerosol scattering and absorption in the atmosphere at different wavelengths. Since AOT was measured directly at the Guangzhou site, we use these data to evaluate the effect of aerosol on the ratio between parameterized $j(NO_2)\downarrow_{param.}$ (Eq. 1) and measured $j(NO_2)\downarrow$ (see Fig. 7). As shown by Garland et al. (2008), the period from 24 to 26 July 2006 was characterized by fresh pollution from the burning of plant waste by local farmers in the vicinity surrounding the measurement site, which is visible in the increased AOT

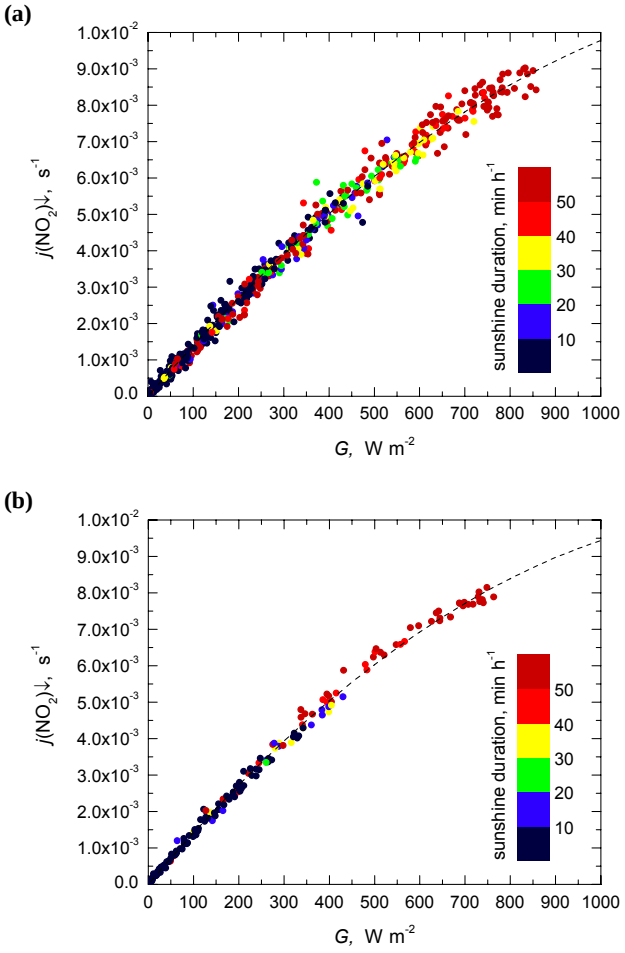

Fig. 6. Scatter plot of $j(NO_2)\downarrow$ versus G (hourly averages) color-coded with the sunshine duration (0–20 min h^{-1}: cloudy sky, 20–40 min h^{-1}: scattered clouds and 40–60 min h^{-1}: fair weather) for **(a)** data from Jülich 2002 and **(b)** data from Hohenpeißenberg 2005. Dashed lines represent the empirical parameterizations for the respective sites from Table 2.

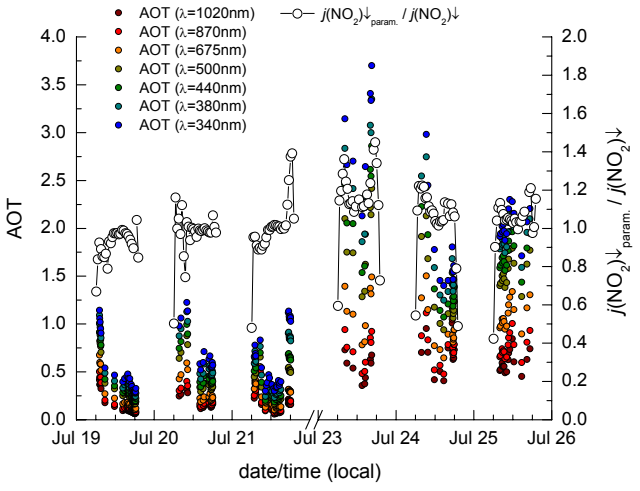

Fig. 7. Time series of AOT and the ratio $j(NO_2)\downarrow_{param.}/j(NO_2)\downarrow$ for the Guangzhou site from 19–21 and 24–26 July 2006. AOT was calculated from sun photometer measurements (Level 2.0, cloud screened and quality-assured) and were obtained from the AERONET (AErosol RObotic NETwork) website (http://aeronet.gsfc.nasa.gov/index.html).

values in Fig. 7. The first three days (19–21 July 2006) with typical pollution were nearly cloud-free, while a few scattered clouds were present during the "intense smoky period". Both midday G and $j(NO_2)\downarrow$ decreased on average by 5–10% from the "typical period" to the "intense smoky period". Figure 7 shows only minor effects on the ratio $j(NO_2)\downarrow_{param.}/j(NO_2)\downarrow$ for both periods. While the performance of our empirical parameterization is generally poorer at sunrise and sunset (as explained in Sect. 3), a slightly increasing trend of $j(NO_2)\downarrow_{param.}/j(NO_2)\downarrow$ is observed during midday with increasing pollution levels. This trend, however, is within the $\pm$10% uncertainty of our parameterization (cf. Fig. 3c).

Obviously, the very polluted atmosphere in Guangzhou (average particle number concentration $\sim$5200 cm^{-3}; D_p=100 nm–10 μm, see Garland et al., 2008) and the less polluted atmosphere in Hohenpeißenberg (average particle number concentration $\sim$2000 cm^{-3}; D_p>10 nm) do not lead to significant differences in Fig. 2. Moreover, results from Brazil during the wet season (average particle number concentration $\sim$400 cm^{-3}; D_p>10 nm, see Guyon et al., 2003) and the dry (biomass burning) season (average particle number concentration $\sim$4000 cm^{-3}) also show only minor differences of $j(NO_2)\downarrow_{param.}/j(NO_2)\downarrow$ that are within the range of those observed in Guangzhou, although AOT values increased by a factor of five to ten from wet season to dry season (not shown). Hence, we could not find evidence from our measurements that the relationship between $j(NO_2)\downarrow$ and G substantially changes with aerosol load, but the potential effect should be kept in mind when using the parameterization.

4.5 Elevation and surrounding terrain

In the troposphere, the downward component of the actinic flux increases with increasing elevation. Thus, the measured $j(NO_2)\downarrow$ values are higher for sites with higher altitude (Marondera and Jungfraujoch, see Fig. 1) due to the decreasing optical thickness of the scattering air masses. The altitude effects on actinic flux are typically much smaller than for irradiance. For example, a calculation with TUV, using the default Elterman aerosol profile, gives a vertical gradient of 1.1%/km for actinic flux and 2.5%/km for irradiance. However, our results suggest (cf. Fig. 1), that the relative increase of UV-A actinic flux with surface elevation is more substantial than that observed for G. Reuder (1999) also showed that the ratio $j(NO_2)\downarrow/G$ is enhanced for sites with an elevation higher than 800 m a.s.l.

The measured $j(NO_2)$ values could be reproduced with the TUV model for each site under clear-sky conditions (exemplarily shown for sites Jarú and Hohenpeißenberg in Fig. 4a and b), except in the cases of Jungfraujoch and Marondera. The Jungfraujoch site is characterized by a complex albedo effect related to distinct topographical patterns, which cannot be reproduced by the TUV model. In addition, the measurement site is substantially higher than the surrounding terrain. The spring measurements at Jungfraujoch in 2001 reveal higher $j(NO_2)\downarrow$ values than the summer measurements (Fig. 1), which is most likely caused by the higher surface albedo of the snow during spring and subsequent atmospheric backscatter.

The measurements at Marondera were made at the end of the dry season when the grass was almost completely withered, such that bare soil (alfisols of granitic origin) was dominating the surface properties. We presume that this dry surface had a much higher albedo in the UV-A range ($\sim$0.1) than typical for grassland ($\sim$0.03) (cf. Feister and Grewe, 1995). According to the TUV model an increase of the surface albedo by 10% raises $j(NO_2)\downarrow$ on average by about 4% (under clear-sky conditions). Using the same input parameters as in Sect. 3 (i.e. $\omega_0 = 0.99$ for relatively non-absorbing aerosols, for example sulfate), a UV-A surface albedo of 0.1 and AOTs ranging from 0.135 to 1.1, the maximum TUV predictions for $j(NO_2)\downarrow$ were about 15–20% lower than revealed by the measurements. Thus we were unable to reproduce the measured data with TUV, except for a UV-A surface albedo of 0.4, which is considered unrealistic.

4.6 Contribution of upwelling $j(NO_2)$

Although $j(NO_2)\downarrow$ can be estimated from G for all sites below 800 m a.s.l. using the polynomial function presented in Sect. 3, it is obvious that upwelling $j(NO_2)$ ($j(NO_2)\uparrow$) would vary substantially from site to site due to the local surface albedo effects. We made measurements of $j(NO_2)\uparrow$ for the sites Jarú (tropical rain forest), Hohenpeißenberg (temperate productive grassland), and Fichtelgebirge (temperate spruce forest). We estimated $j(NO_2)\uparrow$ from our measurements for SZA$< 50°$ in Jarú to 6–8%, in Hohenpeißenberg to 6–8%, and in the Fichtelgebirge to 2–3% of $j(NO_2)\downarrow$. These data should be considered upper limits, because there is typically an unavoidable, slight crosstalk between upper and lower hemispheric measurements. Moreover, local surface effects at the site can influence these measurements. Consequently, the measured upwelling components for Jarú and Hohenpeißenberg are somewhat higher than expected for a typical albedo over vegetation of about 2–3% in the UV-A range (Feister and Grewe, 1995, see Table 1). The surface albedo effect increases $j(NO_2)/G$ (see van der Hage, 1992) and should be considered when the total $j(NO_2)$ (up- and downwelling) are estimated from G. We recommend expanding our empirical function to:

$$j(NO_2) = (1+\alpha) \times \left(B_1 \times G + B_2 \times G^2 \right) \quad (2)$$

where α is the site-dependent UV-A surface albedo. It should be noted that the multiplication by $(1+\alpha)$ is not exactly justified because albedo is defined for irradiance rather than for actinic flux and is therefore only valid for isotropic diffuse radiation. For the direct beam actinic flux the enhancement also depends on the solar zenith angle (Madronich, 1987b). Since we cannot empirically prove the factor $(1+\alpha)$ it should be used with caution. For our sites below 800 m a.s.l., the effect of surface albedo on $j(NO_2)$ is within the uncertainty of the polynomial fit (see α values in Table 1 and Fig. 3c). Large errors could occur if the albedo is high (e.g., above snow) and we recommend that the function should not be used for $\alpha > 0.2$.

4.7 Application to $j(HNO_2)$

Our empirical parameterization can also be applied for the estimation of the HNO_2 photolysis frequency, $j(HNO_2)$, which can be calculated from $j(NO_2)$ with a simple scaling factor. At Jülich, a linear relationship between $j(HNO_2)$ and $j(NO_2)$ was found with a slope of 0.17 (data not shown), and at the Hohenpeißenberg Meteorological Observatory during the SALSA measurement period, a linear relationship was found with a slope of 0.18 (data not shown), both values being comparable to a previous parameterization of Kraus and Hofzumahaus (1998). A small discrepancy can be attributed to the updated molecular data compared to the older NASA-JPL recommendation of 1997 used by Kraus and Hofzumahaus (1998) (see Sect. 2.3). If only G measurements are available we suggest that $j(HNO_2)$ can be approximated using Eq. (2) with $B_1 = 2.65 \times 10^{-6}\,W^{-1}\,m^2\,s^{-1}$ and $B_2 = -8.71 \times 10^{-10}\,W^{-2}\,m^4\,s^{-1}$. In the absence of photolysis frequency measurements, this is a reasonable approach to estimate, for example, the contribution of HNO_2 photolysis to the OH radical production.

5 Conclusions

This paper evaluates side-by-side measurements of downwelling $j(NO_2)$ and solar global irradiance G at nine different field sites. It was found that the relationships are generally non-linear, but very similar for all sites at low to medium altitudes. We thus propose that ground-level $j(NO_2)$ below 800 m a.s.l. can be estimated directly from measured G using an empirical second-order polynomial function. The absolute $j(NO_2)\downarrow$ residual of the empirical function is $\pm 6 \times 10^{-4}\,s^{-1}(2\sigma)$, which corresponds to relative values of $>$40% for $G < 100\,W\,m^{-2}$, 10–40% for $G = 100 - 500\,W\,m^{-2}$ and $\leq$10% for $G > 500\,W\,m^{-2}$. Obviously, it cannot completely replace measurements of $j(NO_2)$ under all conditions and at

all locations. However, in the absence of direct measurements of $j(NO_2)$ the method is more reliable than radiation transfer calculations with poorly known input parameters, in particular in the presence of clouds. The empirical relationship can for example be applied to calculate chemical timescales of the NO-NO_2-O_3 triad in order to evaluate the potential influence of chemical reactions on surface-atmosphere exchange fluxes. Furthermore, the relationship represents a simple tool to evaluate the photochemical steady state (PSS) assumption of NO_x in the absence of $j(NO_2)$ measurements, subsequently being useful for examining the local photochemistry close to the ground. The difference of our estimated $j(NO_2)$ values to previous studies, which proposed a linear relationship between $j(NO_2)$ and G, is up to 50%.

Acknowledgements. The authors gratefully acknowledge financial support by the European Commission (NitroEurope-IP, project 017841), the German Research Foundation (DFG project SALSA, ME 2100/1-1, DFG project EGER, ME 2100/4-1) and by the Max Planck Society. The global radiation data in the Pearl River Delta were collected within the framework of the China National Basic Research and Development Program-2002CB410801. We are indebted to S. Madronich for assistance in using the TUV model and useful hints during the review process. The authors wish to thank K. Staudt and T. Foken from the University of Bayreuth, Micrometeorology Dept. (Germany) for providing solar global irradiance data from the SALSA campaign 2005 and the EGER campaign 2007. We thank the German Meteorological Service (staff of the Meteorological Observatory Hohenpeißenberg, especially C. Plass-Dülmer) for providing HNO_2 photolysis frequency and sunshine duration data. We are also thankful to A. Knaps (FZJ) for providing sunshine duration data during ECHO. We are grateful to K. Hens, M. Kortner, M. Ermel and V. Wolff for helping with some of the measurements in Germany and Switzerland. We thank X. Li and T. Brauers for supervising a spectroradiometer during the PRD 2006 campaign. We are grateful to the principle investigator Po-Hsiung Lin and his staff from the National Taiwan University for establishing and maintaining the AERONET site at Guangzhou during 2006 of which data were used in this study.

The service charges for this open access publication have been covered by the Max Planck Society.

Edited by: R. Martin

References

Acker, K., Möller, D., Wieprecht, W., Meixner, F. X., Bohn, B., Gilge, S., Plass-Dülmer, C., and Berresheim, H.: Strong daytime production of OH from HNO_2 at a rural mountain site, Geophys. Res. Lett., 33, L02809, doi:10.1029/2005GL024643, 2006.

Ammann, C., Flechard, C. R., Leifeld, J., Neftel, A., and Fuhrer, J.: The carbon budget of newly established temperate grassland depends on management intensity, Agr. Ecosyst. Environ., 121, 5–20, 2007.

Andreae, M. O., Artaxo, P., Brandao, C., Carswell, F. E., Ciccioli, P., da Costa, A. L., Culf, A. D., Esteves, J. L., Gash, J. H. C., Grace, J., Kabat, P., Lelieveld, J., Malhi, Y., Manzi, A. O., Meixner, F. X., Nobre, A. D., Nobre, C., Ruivo, M., Silva-Dias, M. A., Stefani, P., Valentini, R., von Jouanne, J., and Waterloo, M. J.: Biogeochemical cycling of carbon, water, energy, trace gases, and aerosols in Amazonia: The LBA-EUSTACH experiments, J. Geophys. Res.-Atmos., 107, 8066, doi:8010.1029/2001JD000524, 2002.

Bahe, F. C., Schurath, U., and Becker, K. H.: The Frequency of NO_2 Photolysis at Ground-Level, as Recorded by a Continuous Actinometer, Atmos. Environ., 14, 711–718, 1980.

Blumthaler, M., Ambach, W., and Salzgeber, M.: Effects of Cloudiness on Global and Diffuse UV Irradiance in a High-Mountain Area, Theor. Appl. Climatol., 50, 23–30, 1994.

Bohn, B.: Solar spectral actinic flux and photolysis frequency measurements in a deciduous forest, J. Geophys. Res.-Atmos., 111, D15303, doi:10.1029/2005JD006902, 2006.

Bohn, B., Corlett, G. K., Gillmann, M., Sanghavi, S., Stange, G., Tensing, E., Vrekoussis, M., Bloss, W. J., Clapp, L. J., Kortner, M., Dorn, H.-P., Monks, P. S., Platt, U., Plass-Dülmer, C., Mihalopoulos, N., Heard, D. E., Clemitshaw, K. C., Meixner, F. X., Prevot, A. S. H., and Schmitt, R.: Photolysis frequency measurement techniques: results of a comparison within the ACCENT project, Atmos. Chem. Phys., 8, 5373–5391, 2008, http://www.atmos-chem-phys.net/8/5373/2008/.

Brauers, T. and Hofzumahaus, A.: Latitudinal Variation of Measured NO_2 Photolysis Frequencies over the Atlantic-Ocean between 50-Degrees-N and 30-Degrees-S, J. Atmos. Chem., 15, 269–282, 1992.

Canada, J., Pedros, G., and Bosca, J. V.: Relationships between UV (0.290–0.385 μm) and broad band solar radiation hourly values in Valencia and Cordoba, Spain, Energy, 28, 199–217, 2003.

Cotte, H., Devaux, C., and Carlier, P.: Transformation of irradiance measurements into spectral actinic flux for photolysis rates determination, J. Atmos. Chem., 26, 1–28, 1997.

Crutzen, P. J., and Lelieveld, J.: Human impacts on atmospheric chemisty, Annu. Rev. Earth Pl. Sc., 29, 17–45, 2001.

Culf, A. D., Esteves, J. L., de O. Marques Filho, A., and Da Rocha, H. R.: Radiation, temperature and humidity over forest and pasture in Amazonia, in: Amazonian Deforestation and Climate, edited by: Gash, J. H. C., Nobre, C. A., Roberts, J. M., and Victoria, R. L., John Wiley, New York, 413–424, 1996.

De Arellano, J. V.-G. and Duynkerke, P. G.: Influence of Chemistry on the Flux-Gradient Relationships for the NO-O_3-NO_2 System, Bound.-Lay. Meteorol., 61, 375–387, 1992.

DeMore, W. B., Sander, S. P., Howard, C. J., Ravishankara, A. R., Golden, D. M., Kolb, C. E., Hampson, R. F., Kurylo, M. J., and Molina, M. J.: Chemical Kinetics and Photochemical Data for Use in Stratospheric Modelling, NASA JPL Publication, 97–4, 1997.

Dickerson, R. R., Stedman, D. H., and Delany, A. C.: Direct Measurements of Ozone and Nitrogen-Dioxide Photolysis Rates in the Troposphere, J. Geophys. Res.-Oc. Atm., 87, 4933–4946, 1982.

Dyer, A. J. and Hicks, B. B.: Flux-Gradient Relationships in the Constant Flux Layer, Q. J. Roy. Meteorol. Soc., 96, 715–721, 1970.

Feister, U. and Grewe, R.: Spectral Albedo Measurements in the UV and Visible Region over Different Types of Surfaces, Photochem. Photobiol., 62, 736–744, 1995.

Fluckiger, E. O.: The High Altitude Research Station Jungfraujoch, 2001 European School of High-Energy Physics, Proceedings (CERN 2002–002), 385–394|xi+401, 2002.

Garland, R. M., Yang, H., Schmid, O., Rose, D., Nowak, A., Achtert, P., Wiedensohler, A., Takegawa, N., Kita, K., Miyazaki, Y., Kondo, Y., Hu, M., Shao, M., Zeng, L. M., Zhang, Y. H., Andreae, M. O., and Pöschl, U.: Aerosol optical properties in a rural environment near the mega-city Guangzhou, China: implications for regional air pollution, radiative forcing and remote sensing, Atmos. Chem. Phys., 8, 5161–5186, 2008, http://www.atmos-chem-phys.net/8/5161/2008/.

Gash, J. H. C. and Nobre, C. A.: Climatic effects of Amazonian deforestation: Some results from ABRACOS, B. Am. Meteorol. Soc., 78, 823–830, 1997.

Gockede, M., Thomas, C., Markkanen, T., Mauder, M., Ruppert, J., and Foken, T.: Sensitivity of Lagrangian Stochastic footprints to turbulence statistics, Tellus B, 59, 577–586, 2007.

Guyon, P., Graham, B., Beck, J., Boucher, O., Gerasopoulos, E., Mayol-Bracero, O. L., Roberts, G. C., Artaxo, P., and Andreae, M. O.: Physical properties and concentration of aerosol particles over the Amazon tropical forest during background and biomass burning conditions, Atmos. Chem. Phys., 3, 951–967, 2003, http://www.atmos-chem-phys.net/3/951/2003/.

Hicks, B. B., Baldocchi, D. D., Meyers, T. P., Hosker, R. P., and Matt, D. R.: A Preliminary Multiple Resistance Routine for Deriving Dry Deposition Velocities from Measured Quantities, Water Air Soil Poll., 36, 311–330, 1987.

Hofzumahaus, A., Kraus, A., and Müller, M.: Solar actinic flux spectroradiometry: a technique for measuring photolysis frequencies in the atmosphere, Appl. Optics, 38, 4443–4460, 1999.

Hofzumahaus, A., Rohrer, F., Lu, K., Bohn, B., Brauers, T., Chang, C.-C., Fuchs, H., Holland, F., Kita, K., Kondo, Y. Li, X., Lou, S., Shao, M., Zeng, L., Wahner, A., and Zhang, Y.: Amplified trace gas removal in the troposphere, Science, 324, 1702–1704, 2009.

Houghton, J. T.: The Physics of Atmospheres, Cambridge University Press, 1986.

Jacovides, C. P., Assimakopoulos, V. D., Tymvios, T. S., Theophilou, K., and Asimakopoulos, D. N.: Solar global UV (280–380 nm) radiation and its relationship with solar global radiation measured on the island of Cyprus, Energy, 31, 2728–2738, 2006.

Kazadzis, S., Bais, A. F., Balis, D., Zerefos, C. S., and Blumthaler, M.: Retrieval of downwelling UV actinic flux density spectra from spectral measurements of global and direct solar UV irradiance, J. Geophys. Res.-Atmos., 105, 4857-4864, 2000.

Kraus, A. and Hofzumahaus, A.: Field measurements of atmospheric photolysis frequencies for O_3, NO_2, HCHO, CH_3CHO, H_2O_2, and HONO by UV spectroradiometry, J. Atmos. Chem., 31, 161–180, 1998.

Kraus, A., Rohrer, F., and Hofzumahaus, A.: Intercomparison of NO_2 photolysis frequency measurements by actinic flux spectroradiometry and chemical actinometry during JCOM97, Geophys. Res. Lett., 27, 1115–1118, 2000.

Kudish, A. I. and Evseev, E.: Statistical relationships between solar UVB and UVA radiation and global radiation measurements at two sites in Israel, Int. J. Climatol., 20, 759–770, 2000.

Kylling, A., Webb, A. R., Bais, A. F., Blumthaler, M., Schmitt, R., Thiel, S., Kazantzidis, A., Kift, R., Misslbeck, M., Schallhart, B., Schreder, J., Topaloglou, C., Kazadzis, S., and Rimmer, J.: Actinic flux determination from measurements of irradiance, J. Geophys. Res.-Atmos., 108(D16), 4506, doi:10.1029/2002JD003236, 2003.

Leighton, P. A.: Photochemistry of Air Pollution, Academic Press, New York and London, 1961.

Lenschow, D. H.: Reactive trace species in the boundary layer from a micrometeorological perspective, J. Meteorol. Soc. Jpn., 60, 161–172, 1982.

Madronich, S.: Intercomparison of NO_2 Photodissociation and UV Radiometer Measurements, Atmos. Environ., 21, 569–578, 1987a.

Madronich, S.: Photodissociation in the Atmosphere: 1. Actinic Flux and the Effects of Ground Reflections and Clouds, J. Geophys. Res.-Atmos., 92, 9740–9752, 1987b.

Mannschreck, K., Gilge, S., Plass-Duelmer, C., Fricke, W., and Berresheim, H.: Assessment of the applicability of NO-NO_2-O_3 photostationary state to long-term measurements at the Hohenpeissenberg GAW Station, Germany, Atmos. Chem. Phys., 4, 1265–1277, 2004, http://www.atmos-chem-phys.net/4/1265/2004/.

McKenzie, R., Johnston, P., Hofzumahaus, A., Kraus, A., Madronich, S., Cantrell, C., Calvert, J., and Shetter, R.: Relationship between photolysis frequencies derived from spectroscopic measurements of actinic fluxes and irradiances during the IPMMI campaign, J. Geophys. Res.-Atmos., 107(D5), 4042, 10.1029/2001JD000601, 2002.

Meixner, F. X., Fickinger, T., Marufu, L., Serca, D., Nathaus, F. J., Makina, E., Mukurumbira, L., and Andreae, M. O.: Preliminary results on nitric oxide emission from a southern African savanna ecosystem, Nutr. Cycl. Agroecosys., 48, 123–138, 1997.

Merienne, M. F., Jenouvrier, A., and Coquart, B.: The NO_2 Absorption-Spectrum .1. Absorption Cross-Sections at Ambient-Temperature in the 300–500 Nm Region, J. Atmos. Chem., 20, 281–297, 1995.

Monks, P. S., Rickard, A. R., Hall, S. L., and Richards, N. A. D.: Attenuation of spectral actinic flux and photolysis frequencies at the surface through homogenous cloud fields, J. Geophys. Res.-Atmos., 109, D17206, doi:10.1029/2003JD004076, 2004.

Niemela, S., Raisanen, P., and Savijarvi, H.: Comparison of surface radiative flux parameterizations – Part II. Shortwave radiation, Atmos, Res,, 58, 141–154, 2001.

Ogunjobi, K. O. and Kim, Y. J.: Ultraviolet (0.280–0.400 μm) and broadband solar hourly radiation at Kwangju, South Korea: analysis of their correlation with aerosol optical depth and clearness index, Atmos. Res., 71, 193–214, 2004.

Paltridge, G. W. and Platt, C. M. R.: Radiative Processes in Meteorology and Climatology, Elsevier, Amsterdam, 318 pp., 1976.

Parrish, D. D., Murphy, P. C., Albritton, D. L., and Fehsenfeld, F. C.: The Measurement of the Photo-Dissociation Rate of NO_2 in the Atmosphere, Atmos. Environ., 17, 1365–1379, 1983.

Reuder, J.: Untersuchungen zur Variabilität von Photolysefrequenzen, "Aktuelle Reihe" der Brandenburgischen Technischen Universität Cottbus, Fakultät Umweltwissenschaften und Verfahrenstechnik, BTUC-AR 4/99, ISSN 1434-6834, 1999.

Ruggaber, A., Forkel, R., and Dlugi, R.: Spectral Actinic Flux and Its Ratio to Spectral Irradiance by Radiation Transfer Calculations, J. Geophys. Res.-Atmos., 98, 1151–1162, 1993.

Rummel, U., Ammann, C., Gut, A., Meixner, F. X., and Andreae, M. O.: Eddy covariance measurements of nitric oxide flux within

an Amazonian rain forest, J. Geophys. Res.-Atmos., 107(D20), 8050, doi:10.1029/2001JD000520, 2002.

Rummel, U., Ammann, C., Kirkman, G. A., Moura, M. A. L., Foken, T., Andreae, M. O., and Meixner, F. X.: Seasonal variation of ozone deposition to a tropical rain forest in southwest Amazonia, Atmos. Chem. Phys., 7, 5415–5435, 2007, http://www.atmos-chem-phys.net/7/5415/2007/.

Schallhart, B., Huber, A., and Blumthaler, M.: Semi-empirical method for the conversion of spectral UV global irradiance data into actinic flux, Atmos. Environ., 38, 4341–4346, 2004.

Schere, K. L. and Demerjian, K. L.: A photochemical box model for urban air quality simulations, in: Proceedings of the Fourth Joint Conference on Sensing of Environmental Pollutants, American Chemical Society, 1978.

Seinfeld, J. H. and Pandis, S. N.: Atmospheric Chemistry and Physics: From Air Pollution to Climate Change, John Wiley & Sons, Inc., New York, 2006.

Shetter, R. E., Junkermann, W., Swartz, W. H., Frost, G. J., Crawford, J. H., Lefer, B. L., Barrick, J. D., Hall, S. R., Hofzumahaus, A., Bais, A., Calvert, J. G., Cantrell, C. A., Madronich, S., Muller, M., Kraus, A., Monks, P. S., Edwards, G. D., McKenzie, R., Johnston, P., Schmitt, R., Griffioen, E., Krol, M., Kylling, A., Dickerson, R. R., Lloyd, S. A., Martin, T., Gardiner, B., Mayer, B., Pfister, G., Roth, E. P., Koepke, P., Ruggaber, A., Schwander, H., and van Weele, M.: Photolysis frequency of NO_2: Measurement and modeling during the International Photolysis Frequency Measurement and Modeling Intercomparison (IPMMI), J. Geophys. Res.-Atmos., 108(D16), 8544, doi:10.1029/2002JD002932, 2003.

Sutton, M. A., Nemitz, E., Erisman, J. W., Beier, C., Bahl, K. B., Cellier, P., de Vries, W., Cotrufo, F., Skiba, U., Di Marco, C., Jones, S., Laville, P., Soussana, J. F., Loubet, B., Twigg, M., Famulari, D., Whitehead, J., Gallagher, M. W., Neftel, A., Flechard, C. R., Herrmann, B., Calanca, P. L., Schjoerring, J. K., Daemmgen, U., Horvath, L., Tang, Y. S., Emmett, B. A., Tietema, A., Penuelas, J., Kesik, M., Brueggemann, N., Pilegaard, K., Vesala, T., Campbell, C. L., Olesen, J. E., Dragosits, U., Theobald, M. R., Levy, P., Mobbs, D. C., Milne, R., Viovy, N., Vuichard, N., Smith, J. U., Smith, P., Bergamaschi, P., Fowler, D., and Reis, S.: Challenges in quantifying biosphere-atmosphere exchange of nitrogen species, Environ. Pollut., 150, 125–139, 2007.

Thielmann, A., Prevot, A. S. H., Gruebler, F. C., and Staehelin, J.: Empirical ozone isopleths as a tool to identify ozone production regimes, Geophys. Res. Lett., 28, 2369–2372, 2001.

Tomasi, C., Vitale, V., and De Santis, L. V.: Relative optical mass functions for air, water vapour, ozone and nitrogen dioxide in atmospheric models presenting different latitudinal and seasonal conditions, Meteorol. Atmos. Phys., 65, 11–30, 1998.

Trebs, I., Lara, L. S., Zeri, L. M., Gatti, L. V., Artaxo, P., Dlugi, R., Slanina, J., Andreae, M. O., and Meixner, F. X.: Dry and wet deposition of atmospheric inorganic nitrogen in a tropical environment (Rondônia, Brazil), Atmos. Chem. Phys., 6, 447–469, 2006, http://www.atmos-chem-phys.net/6/447/2006/.

Troe, J.: Are primary quantum yields of NO_2 photolysis at $\lambda = 398$ nm smaller than unity?, Z. Phys. Chem., 214, 573–581, 2000.

Van der Hage, J. C. H.: Actinic Flux and Global Radiation, Theor. Appl. Climatol., 46, 173–177, 1992.

van Weele, M., De Arellano, J. V., and Kuik, F.: Combined Measurements of UV-A Actinic Flux, UV-A Irradiance and Global Radiation in Relation to Photodissociation Rates, Tellus B, 47, 353–364, 1995.

Volz-Thomas, A., Lerner, A., Patz, H. W., Schultz, M., McKenna, D. S., Schmitt, R., Madronich, S., and Roth, E. P.: Airborne measurements of the photolysis frequency of NO_2, J. Geophys. Res.-Atmos., 101, 18613–18627, 1996.

Webb, A. R., Bais, A. F., Blumthaler, M., Gobbi, G. P., Kylling, A., Schmitt, R., Thiel, S., Barnaba, F., Danielsen, T., Junkermann, W., Kazantzidis, A., Kelly, P., Kift, R., Liberti, G. L., Misslbeck, M., Schallhart, B., Schreder, J., and Topaloglou, C.: Measuring spectral actinic flux and irradiance: Experimental results from the Actinic Flux Determination from Measurements of Irradiance (ADMIRA) project, J. Atmos. Ocean. Tech., 19, 1049–1062, 2002a.

Webb, A. R., Kift, R., Thiel, S., and Blumthaler, M.: An empirical method for the conversion of spectral UV irradiance measurements to actinic flux data, Atmos. Environ., 36, 4397–4404, 2002b.

Webb, A. R.: UV instrumentation for field and forest research, Agr. Forest Meteorol., 120, 27–38, 2003.

Wiegand, A. N. and Bofinger, N. D.: Review of empirical methods for the calculation of the diurnal NO_2 photolysis rate coefficient, Atmos. Environ., 34, 99–108, 2000.

Winkler, P.: Geschichte der Meteorologie in Deutschland: Hohenpeißenberg 1781–2006 – das Älteste Bergobservatorium der Welt Deutscher Wetterdienst, Offenbach am Main, 2006.

Wratt, D. S., Hadfield, M. G., Jones, M. T., Johnson, G. M., and McBurney, I.: Power Stations, Oxides of Nitrogen Emissions, and Photochemical Smog – a Modeling Approach to Guide Decision Makers, Ecol. Model., 64, 185–203, 1992.

Yang, J., Honrath, R. E., Peterson, M. C., Parrish, D. D., and Warshawsky, M.: Photostationary state deviation-estimated peroxy radicals and their implications for HO_x and ozone photochemistry at a remote northern Atlantic coastal site, J. Geophys. Res.-Atmos., 109, D02312, doi:10.1029/2003JD003983, 2004.

Zafonte, L., Rieger, P. L., and Holmes, J. R.: Nitrogen Dioxide Photolysis in Los-Angeles Atmosphere, Environ. Sci. Technol., 11, 483–487, 1977.